Journal of Microbiology (2013) Vol. 51, No. 5, pp. 627–632
DOI 10.1007/s12275-013-3234-2

Crystal Structure of XoLAP, a Leucine Aminopeptidase, from *Xanthomonas oryzae* pv. *oryzae*[§]

Jin-Kwang Kim[1†], Sampath Natarajan[1†], Hanseul Park[2], Kim-Hung Huynh[1], Sang Hee Lee[3], Jeong-Gu Kim[4], Yeh-Jin Ahn[2*], and Lin-Woo Kang[1,5*]

[1]*Department of Biological Sciences, Konkuk University, Seoul 143-701, Republic of Korea*
[2]*Department of Green Life Science, College of Convergence, Sangmyung University, Seoul 110-743, Republic of Korea*
[3]*Drug Resistance Proteomics Laboratory, Department of Biological Sciences, Myongji University, Yongin 449-728, Republic of Korea*
[4]*Microbial Genetics Division, National Institute of Agricultural Biotechnology (NIAB), Rural Development Administration (RDA), Suwon 441-707, Republic of Korea*
[5]*Protein and Chemical Inc., Seoul 143-701, Republic of Korea*

(Received April 22, 2013 / Accepted May 17, 2013)

Aminopeptidases are metalloproteinases that degrade N-terminal residues from protein and play important roles in cell growth and development by controlling cell homeostasis and protein maturation. We determined the crystal structure of XoLAP, a leucyl aminopeptidase, at 2.6 Å resolution from *Xanthomonas oryzae* pv. *oryzae*, causing the destructive rice disease of bacterial blight. It is the first crystal structure of aminopeptidase from phytopathogens as a drug target. XoLAP existed as a hexamer and the monomer structure consisted of an N-terminal cap domain and a C-terminal peptidase domain with two divalent zinc ions. XoLAP structure was compared with BlLAP and EcLAP (EcPepA) structures. Based on the structural comparison, the molecular model of XoLAP in complex with the natural aminopeptidase inhibitor of microginin FR1 was proposed. The model structure will be useful to develop a novel antibacterial drug against Xoo.

***Keywords*:** aminopeptidase, *Xanthomonas oryzae* pv. *oryzae* (Xoo), microginin FR1, crystal structure, drug target

Introduction

Xanthomonas oryzae pv. *oryzae* (Xoo), a phytopathogen, is responsible for bacterial blight (BB), a destructive disease that results in significant production losses of rice worldwide, particularly in Asia (Zhang and Wang, 2013). This fatal vascular disease causes systemic infections in rice leaves, resulting in the formation of tannish grey to white lesions along the veins, and thus far no effective drug has been developed. In 2005, Lee and coworkers described the complete genome of Xoo, which has been used to identify target genes for antibacterial drug development against BB (Lee *et al*., 2005). We selected approximately 100 putative drug target proteins (Payne *et al*., 2007; Kim *et al*., 2011, 2013), important for the bacterial survival, which includes a leucine aminopeptidase (LAP) encoded by the gene *XoLAP* (*Xo0834*).

Aminopeptidase (AP), a member of diverse exopeptidase families, plays important roles in cell maintenance, growth, development, and defense by controlling protein maturation and stability (Botbol and Scronik, 1991; Matsui *et al*., 2006). AP hydrolyzes N-terminal amino acids from short peptides ranging from 15 to 50 residues, and many disease states are associated with the impaired proteolytic function (Taylor, 1993). Leucyl aminopeptidase (LAP; EC 3.4.11.1) is a cytosolic enzyme that catalyzes removal of leucine residues from the N-termini of proteins and peptides. LAPs often have broader substrate specificity and hydrolyze other amino acids such as N-terminal methionine, phenylalanine, or isoleucine residues. LAPs are classified into M1 and M17 families based on sequence similarity (Rawlings *et al*., 2006). Each LAP family exhibits distinct geometrical and functional features. M17 LAPs form a hexamer consisting of six identical monomers, with each monomer possessing two metal ions in its active site (Rawlings and Barrett, 1996; Rawlings *et al*., 2006). In contrast, M1 family LAPs consist of a single monomer and contain a single metal ion in their active site, along with the specific metallopeptidase motif HEXXH, which is not present in M17 LAPs. XoLAP belongs to the M17 family based on the amino acid sequence. Among the M17 family, several LAPs including *E. coli* PepA (EcPepA) has an additional DNA-binding activity in the N-terminal domain, and works as transcriptional repressors for controlling pyrimidine, alginate, and cholera toxin biosynthesis, and even mediate site-specific recombination events in the naturally occurring multicopy plasmids (e.g. *cer* from ColE1 and *psi* from pSC101) (Stirling *et al*., 1989; Charlier *et al*., 1995; Alen *et al*., 1997).

Recently, aminopeptidases have been emerged as promising new drug targets for the development of antibacterial drugs, based on the essential role of protein maturation and stability (Lu *et al*., 2012; Sivaraman *et al*., 2012), and the inhibitors are being developed. Herein, we determined the crystal structure of XoLAP and analyzed the DNA-binding activity of the N-terminal domain *in vitro* and the peptidase active site structure of the C-terminal domain. It is the first crystal

[†] These authors contributed equally to this work.
*For correspondence. (L.W. Kang) E-mail: lkang@konkuk.ac.kr; Tel.: +82-2-450-4090; Fax: +82-2-444-6707 / (Y.J. Ahn) E-mail: yjahn@smu.ac.kr; Tel.: +82-2-2287-5483; Fax: +82-2-2287-0070
[§]Supplemental material for this article may be found at http://www.springerlink.com/content/120956.

structure of LAP from phytopathogens. The natural inhibitor, microginin FR1 (Kraft *et al.*, 2006; Neumann *et al.*, 2006), bound XoLAP model was also proposed.

Materials and Methods

Purification and crystallization of XoLAP

XoLAP was expressed and purified from *E. coli* as described previously (Huynh *et al.*, 2009). Briefly, *XoLAP* gene was cloned from Xoo genomic DNA to our modified pET11a-TEV vector (Doan *et al.*, 2008) and XoLAP protein was over-expressed in *E. coli* strain BL21(DE3) cells at 295K by the addition of isopropyl-β-D-thiogalactopyranoside (IPTG) to a final concentration of 0.5 mM at OD_{600} of 0.6 in Luria-Bertani medium. XoLAP was expressed with an extra 18 residues of MGHHHHHHSSENLYFQGH at its N-terminus from the expression vector and after TEV cleavage only two residues of GH remaining at the N-terminus. The cultured cells were harvested and resuspended in ice-cold lysis buffer (25 mM Tris-HCl; pH 7.5, 300 mM NaCl, 15 mM Imidazole, and 3 mM β-mercaptoethanol) and homogenized with a sonicator (Sonomasher, S & T Science, Korea). The soluble fraction of crude cell extract was purified by Ni-NTA resin column (Qiagen) using the washing buffer [25 mM Tris-HCl; pH 7.5, 1 M NaCl, 3 mM β-mercaptoethanol, 40 mM imidazole, and 20% (v/v) glycerol] and the elution buffer [25 mM Tris-HCl; pH 7.5, 300 mM NaCl, 200 mM imidazole, 3 mM β-mercaptoethanol, and 20% (v/v) glycerol]. The resulting protein solution was treated with TEV protease at 277K for overnight to cut the affinity tag, and applied to a Superdex 75 prep-grade column, which was previously equilibrated with the buffer [25 mM Tris-HCl; pH 7.5, 150 mM NaCl, and 3 mM β-mercaptoethanol]. The homogeneity of the eluted XoLAP protein was extensively dialyzed with the buffer containing 25 mM Tris-HCl; pH 7.5, 3 mM β-mercaptoethanol, 20% (v/v) glycerol, and followed by concentration to 10 mg/ml. XoLAP crystals were grown at 298K under the conditions of 0.05 M $CaCl_2 \cdot H_2O$ 0.1 M Bis-Tris; pH 6.5, and 30% PEG monomethyl ether 550 by the hanging drop vapor diffusion method in several weeks. For data collection, a crystal was cryoprotected in liquid nitrogen with 25% (v/v) glycerol as a cryoprotectant.

Table 1. Data collection statistics

Parameters	XoLAP
Space group	$P2_13$
Cell constant (Å/ °)	
$a = b = c$	152.1
$\alpha = \beta = \gamma$	90.0
Synchrotron	PLS BL-6C1
Wavelength (Å)	0.96418
Resolution Range (Å)	50.0–2.6 (2.64–2.60)
Completeness (%)	100.0 (100.0)
Molecules per AU	2
No. non-hydrogen	7799
No. of waters	704
R_{work}/ R_{free} (%)	14.6 / 21.5
RMSD bond lengths/angles (Å/°)	0.017/1.71
Average B-factor (Å^2)	25.7
Ramachandran plot (%)	95.9/3.59/0.51

* $R_{sym} = \Sigma_h\Sigma_i|I(h)_i - <I(h)>|/\Sigma_h\Sigma_i I(h)_i$, where $I(h)$ is the intensity of reflection h, Σ_h is the sum over all reflections, and Σ_i is the sum over i measurements of reflection h.
Values in parentheses correspond to the last resolution shell.
Values of Ramachandran plot (%) represent the favored, allowed, and generously allowed regions, respectively.

Structure determination

X-ray diffraction data were collected from the flash cooled crystal using a Bruker Proteum 300 CCD detector on beamline 6C1 at Pohang Light Source (PLS), Republic of Korea (Table 1). The XoLAP crystal belonged to cubic space group $P2_13$ with cell dimensions of $a = b = c = 152.1$ Å and contained two monomers in its asymmetric unit. The programs DENZO and SCALEPACK were used for data reduction (Otwinowski and Minor, 1997). The structure model of XoLAP was determined by molecular replacement (MR) using the MOLREP program (Vagin and Teplyakov, 2010) with the crystal structure of EcLAP (PepA from *E. coli*) (PDB code 1GYT) (Strater *et al.*, 1999) as a search model, which shares 48.3% sequence identity with XoLAP. The model was built using the COOT program (Emsley and Cowtan, 2004) and refined using Refmac5 (Murshudov *et al.*, 1997). The final model (PDB ID: 3JRU) was deposited in the Protein Data Bank (PDB) (Table 1). Model quality and stereochemistry were evaluated using PROCHECK (Laskowski *et al.*, 1993). Comparisons between XoLAP and other LAP structures from *E. coli* and bovine lens, and presentations of molecular surfaces, electrostatic potentials, and figures were computed using PyMOL (Delano, 2002). Molecular interactions between protomers in hexamer were calculated using the programs of accessible surface areas and molecular contacts analysis in CCP4 program suite (CCP4, 1994).

EMSA (electrophoretic mobility shift assay)

The plasmids of p-*cer*^{2} and p-*psi*^{2}, and pUC19 (Reijns *et al.*, 2005) were obtained from Dr. Sean Colloms at University of Glasgow. The plasmid of pUC19, which do not have *cer* and *psi* sites, was used for negative control for the EMSA experiment. The DNA-binding reaction was carried out at 20°C for 4 h in 10 ml of reaction buffer (25 mM Tris-HCl; pH 7.5, 60 mM KCl, 3 mM β-mercaptoethanol, 2.5% glycerol, 5 mM MgCl, 0.5% NP-40, 0.2 mM EDTA) including 0.5 mM purified plasmid DNA and various concentrations (0–50 mM) of XoLAP protein. The reaction mixtures were subjected to native gel electrophoresis (NativePAGE^{TM} 3–12% Bis-Tris Gel, 1.0 mm × 10 well, Invitrogen, USA) after pre-running at 4°C. DNA fragments were visualized with EtBr staining.

Results and Discussion

XoLAP hexamer structure

The crystal structure of XoLAP was determined at 2.6 Å resolution (Fig. 1A). The XoLAP crystal contained two complete monomers in its asymmetric unit (Fig. 1B). Details of the structure statistics are presented in Table 1. XoLAP has 32 symmetry, with three dimers in threefold symmetry, for-

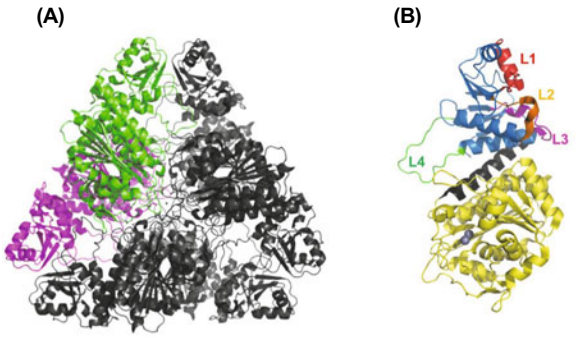

Fig. 1. The cartoon diagram of XoLAP structure. (A) The hexameric structure of XoLAP. Dimer in asymmetric unit was represented by colors as green and magenta. Hexameric structure was generated by symmetry. (B) The monomeric structure of XoLAP with two Zn ions (grey sphere). N-terminal domain is shown in light blue, and C-terminal domain is in yellow. Four loops (L1-L4) in N-terminal domain are colored in red (L1), orange (L2), magenta (L3), and green (L4). The connecting long α-helix between domains of N-terminal and C-terminal is indicated by dark grey color.

ming the hexamer geometry. Overall XoLAP hexamer structure was similar to the previously reported LAP structures of EcLAP (Strater *et al*., 1999) and BlLAP (Burley *et al*., 1990), having a triangular shape with an edge length of approximately 135 Å. The total buried surface of XoLAP monomer upon hexamerization is 4061 Å^2, about 21% of the solvent accessible surface area of 14928 Å^2. Among 21% of the buried surface, 15% is located in dimer interface and 6% interacts with other three monomers. Therefore, only two monomers in hexamer do not have contacts with each other. Most interactions in the interfaces are van der Waals interactions rather than H-bond interactions (Supplementary data Table S1). Six catalytic domains were clustered at the core of the hexamer, where they pack around a central threefold axis and stabilize the trimer-to-trimer packing. A large solvent cavity of ~15 Å radius and ~10 Å thickness was formed at the center of the hexamer, which harbored the aminopeptidase active site. Each corner of the triangle was extended by N-terminal domains, which are mainly responsible for DNA-inding activity in several LAPs.

XoLAP monomer structure

All 490 residues were included in the structure refinement. The XoLAP monomer consists of two domains (an N-terminal DNA-binding domain and a C-terminal peptidase domain) connected by a long α-helix (residues 165–188) (Fig. 1B). The C-terminal domain (residues 194–490) contains an αbα motif composed of a central eight-stranded mixed (parallel/anti-parallel) β-sheet surrounded by six or five α-helices on each side. Additionally, a small two-stranded β-sheet was observed at the interface between the C-terminal domains, which assists in hexamer oligomerization. The aminopeptidase active site is located in the C-terminal domain and contains two divalent zinc metal ions and one bicarbonate anion. The smaller N-terminal domain (residues 1–164) is composed of a six-stranded mixed (parallel/anti-parallel) β-sheet flanked by two or three α-helices on each side. Among these, three of the β-sheets are capped by two α-helices on the top, while the other three are shielded by a helix and loops. The C- and N-terminal domains of XoLAP are in different orientations, and the N-terminal domain is tilted at approximately 39° with respect to the C-terminal domain.

Analysis of the overall B-factors of the XoLAP structure showed that the N-terminal domain had significantly higher thermal motion than the C-terminal domain. This higher temperature factor indicates that the residues of the N-terminal domains were more flexible. Mostly atoms with high B-factor were observed in the loop regions of the N-terminal domain. The long loop (L4; residues 140–156) in the N-terminal domain showed the highest average B-factor (56.3 Å^2).

Table 2. Detail structure comparison of XoLAP with EcLAP and BlLAP (overall and N- and C-terminal domains alone) and their corresponding RMSD (Å)

XoLAP vs.	Whole structure RMSD (Å)	Residue Nos.	N-terminal RMSD (Å)	Residue Nos.
EcLAP	1.50	1-163	1.16	193–503
BlLAP	1.86	1-163	2.82	193–486

Structure comparison with other LAPs

Multiple sequence alignment (MSA) analyses of *Escherichia coli* LAP (EcLAP, P11648) (Strater *et al*., 1999), *Vibrio cholera* LAP (VcLAP, AAF91462), *Salmonella typhimurium* LAP (StLAP, NP_463337), bovine lens LAP (BlLAP, P00727) (Burley *et al*., 1990), *Pseudomonas aeruginosa* LAP (PaLAP), *Haemophilus influenzae* LAP (HiLAP), and Xoo LAP (XoLAP, YP_199473) were carried out (Fig. 2). Overall N-terminal domain sequences were more various than C-terminal domain, of which the metal-binding five residues were completely conserved. It shows the functional importance of divalent metal ions in the peptidase activity. Pairwise sequence alignment found that XoLAP shares 48.3% sequence identity with EcLAP and 34.9% with BlLAP, and structural comparison of XoLAP with EcLAP and BlLAP showed root mean square deviation (RMSD) values of 1.50 Å and 1.86 Å, respectively (Table 2). Conformations of N-terminal and C-terminal domains were also different. Although EcLAP N-terminal domain was tilted at approximately 37° with respect to C-terminal domain, which is similar with XoLAP, BlLAP N-terminal domain was tilted only at 27° and two domains packed more tightly to each other. There was also difference in the domain-connecting helix, which was longer and slightly bent towards the N-terminal domain in EcLAP: in XoLAP, this helix was straight and shorter, and similar to that of BlLAP in length.

N-terminal putative DNA-binding domain

EcLAP, also known as EcPepA, has DNA-binding/recombination activity for *cer* and *psi* sites in naturally occurring multicopy plasmids (Reijns *et al*., 2005), and the N-terminal domain of EcLAP, especially three loops of L1, L2, and L3, are essential for the DNA binding (Strater *et al*., 1999). Site-directed mutation study in EcLAP showed total 30 residues related to the DNA recombination activity, of which 25 residues were located in the N-terminal domain and remaining five residues in the C-terminal domain (Reijns *et al*., 2005) (Fig. 2 and Supplementary data Fig. S1A). XoLAP structure

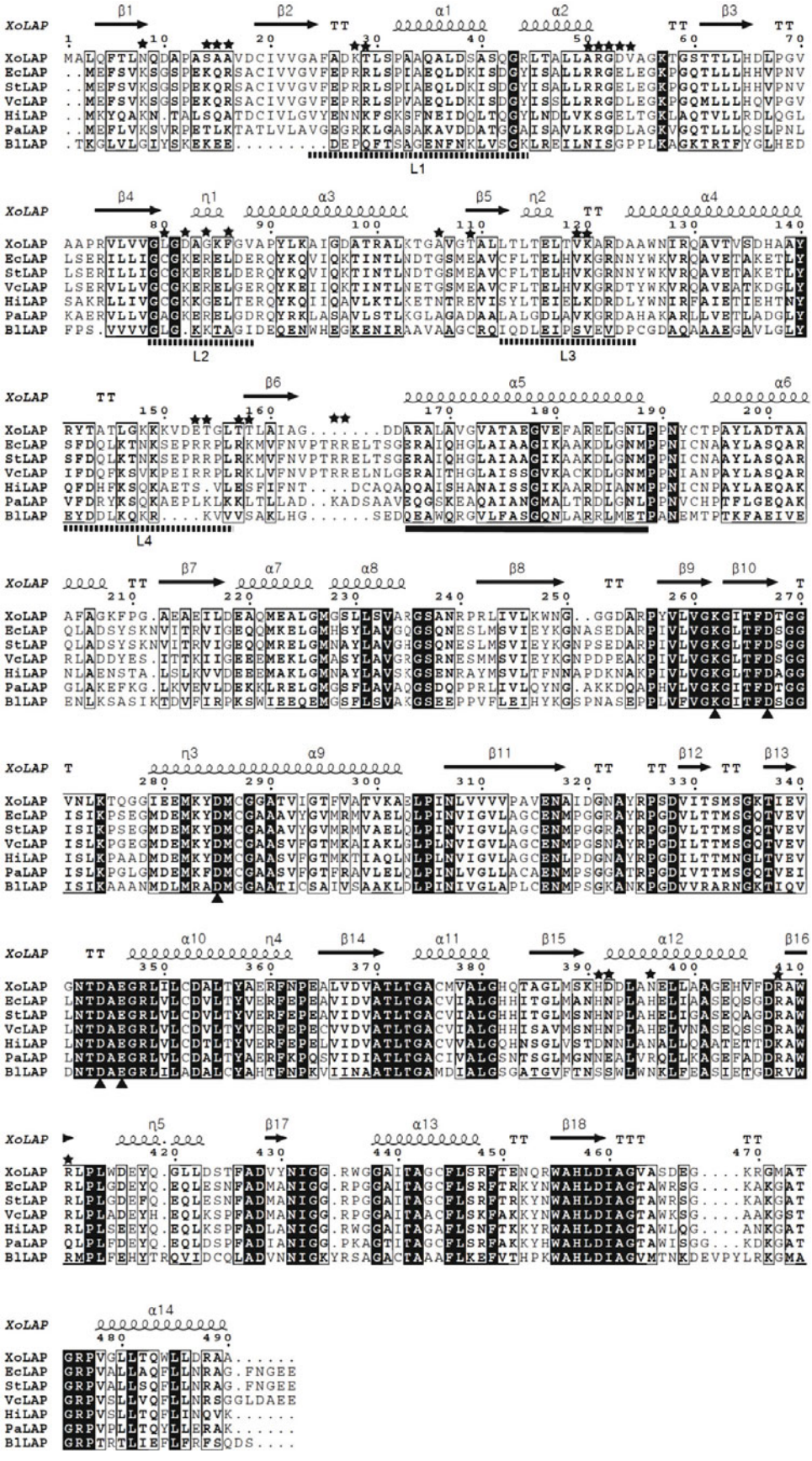

Fig. 2. Multiple sequence alignment of LAP structures from various species. The proteins listed from top to bottom: XoLAP from *X. oryzae* pv. *oryzae*; EcLAP from *E. coli*; StLAP from *S. typhimurium*; VcLAP from *V. cholera*; HiLAP from *H. influenza*; PaLAP from *P. aeruginosa*; BlLAP from bovine lens. Fully conserved residues shown in black boxes with white character and partially conserved residues shown in boxes with bold characters. Secondary structures of helix, sheet and turn for XoLAP structure are shown in the top of the sequences. The corresponding regions of EcLAP L1, L2, L3, and L4 are marked as dashed black bars in the bottom of the sequences. EcLAP L1, L2, and L3 are responsible for its DNA binding activity. The black solid bar indicates the long helix connecting the N-terminal and C-terminal domains. Black triangles represent the conserved metal-binding residues and black stars represent putative DNA-binding residues in EcLAP.

corresponding to the three loops was more similar to EcLAP rather than BlLAP (Supplementary data Fig. S1B). In EcLAP, 18 of the 25 amino acids were basic amino acids. In XoLAP, only six amino acids were basic amino acids among the corresponding 25 residues. Two of five amino acids in the C-terminal domain of EcLAP were basic amino acids, which were also conserved in XoLAP. In order to estimate the DNA-binding activity of XoLAP, EMSA experiments were performed with p-*cer*[2] and p-*psi*[2] plasmids (Reijns *et al*., 2005). We could not detect *in vitro* DNA-binding of XoLAP for both plasmids even with hundred-fold higher amount of XoLAP (Supplementary data Fig. S2). We speculate the fewer number of basic residues at the putative XoLAP DNA-binding sites could lessen the DNA-binding affinity. In EcLAP, the direct repeat of recognition sites and the supercoiled conformation of target DNA affect the DNA binding, and for the site-specific DNA recombination activity other accessory proteins such as ArgR, XerC, and XerD are also required. Therefore, various other factors than XoLAP could affect the DNA binding.

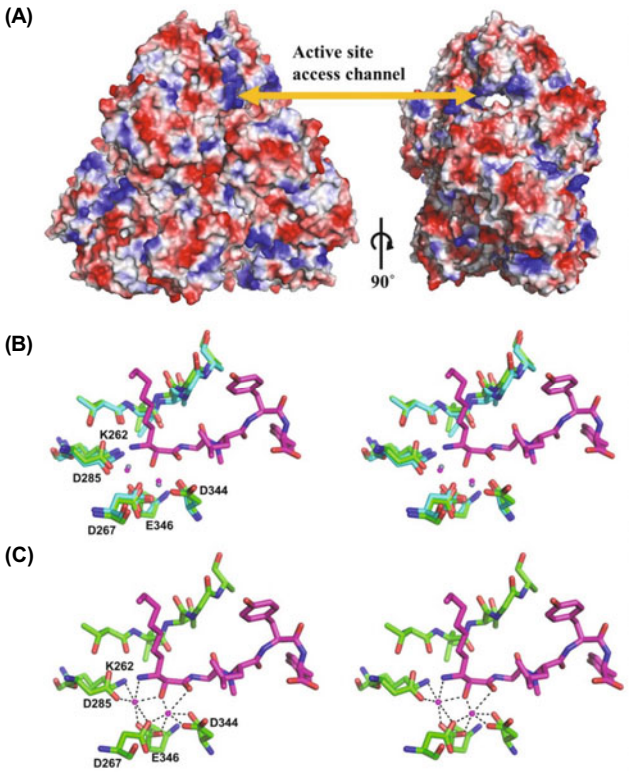

Fig. 3. Electrostatic molecular surface and microginin FR1-bound model of XoLAP. (A) Electrostatic potential surface of XoLAP hexamer. The colors of red, blue, and white represent the residues of negative, positive, and hydrophobic nature on the surface. One of three active site access channels is marked as an orange arrow. Right figure shows in 90° rotation view. (B) Stereo representation of superimposed active site residues of BlLAP (cyan) and XoLAP (green) with metal ions and the inhibitor microginin FR1 (purple). (C) Stereo microginin FR1-bound XoLAP model with metal coordinations. Dotted lines indicate the coordinations of two metal ions.

Active site of C-terminal peptidase domain

Access to the XoLAP active site cavity can be achieved through three possible channels, located along the twofold molecular axis at the interface between the two N-terminal and two C-terminal domains (Fig. 3A). The entrances to the channels are occupied by positively charged residues, and the channels allowed access to the central hexamer cavity. Each XoLAP monomer has two metal-binding sites, and each site contains a divalent Zn ion (Supplementary data Fig. S3). In monomer A, both metal ions Zn1 and Zn2 are penta-coordinated in a distorted pyramidal geometry. In monomer B, a water molecule exists at the bridging position between two Zn ions, whereas there is no water at the corresponding position in monomer A. Accordingly, Zn1 in monomer B has six coordination bonds. Of the two Zn ions, Zn1 achieves tighter binding with the shorter bond distances by more negatively charged residues. Metal-coordinating atoms include carboxylic oxygen atoms from four negatively charged residues (D267, D285, D344, and E346), and an additional coordination bond originate from the side chain amino group of K262. A water molecule, observed at the bridging position in chain B, produces tight coordination bonding (2.6 Å) to Zn1 and loose coordination bonding (3.7 Å) to Zn2. As reported for other LAP structures, a bicarbonate ion, acting as a catalytic base, is also observed near the XoLAP active site. This bicarbonate ion shows three hydrogen bond interactions with the guanidine and amino groups of R348.

We superimposed BlLAP structure in complex with the natural inhibitor of microginin FR1 with XoLAP in order to compare the substrate binding pocket and the active site geometry including two Zn binding sites (Fig. 3B). The structure of XoLAP active site was well superimposed with that of BlLAP, and from the structural comparison, microginin FR1-bound XoLAP model was proposed (Fig. 3C). The model showed both metal ions were coordinated with octahedral geometry by K262, D267, D285, D344, and E346 at the distances from 1.7 Å to 3.0 Å and the oxygen atom at the center position of microginin FR1 bridged the two metal ions, as shown in the BlLAP complex structure. No steric hindrance was observed between the bound microginin FR1 and XoLAP active site residues. This inhibitor bound model will be useful to develop a novel inhibitor against XoLAP.

Acknowledgements

We are thankful for two multicopy plasmids, p-*cer*[2] and p-*psi*[2], for DNA-recombination assay from Dr. Sean Colloms at University of Glasgow. We are grateful to staff members for their assistance with the beamline BL-6C1 at Pohang Light Source (PLS), Republic of Korea. This work was supported by grants from the Next-Generation BioGreen 21 Program (No. PJ009500 and PJ009082), Rural Development Administration, Republic of Korea, and by the Korean Research Foundation (NRF) grant funded by the Korean government (MEST) (No. 2012-0008737), and by the Marine and Extreme Genome Research Center Program of the Ministry of Land, Transportation and Maritime Affairs, Republic of Korea.

References

Alen, C., Sherratt, D.J., and Colloms, S.D. 1997. Direct interaction of aminopeptidase A with recombination site DNA in Xer site-specific recombination. *EMBO J.* **16**, 5188–5197.

Botbol, V. and Scronik, O.A. 1991. Measurement of instant rates of protein degradation in the livers of intact mice by the accumulation of bestatin-induced peptides. *J. Biol. Chem.* **266**, 179–186.

Burley, S.K., David, P.R., Taylor, A., and Lipscomb, W.N. 1990. Molecular structure of leucine aminopeptidase at 2.7-A resolution. *Proc. Natl. Acad. Sci. USA* **87**, 6878–6882.

CCP4. 1994. The CCP4 suite: programs for protein crystallography. *Acta. Crystallogr. D Biol. Crystallogr.* **50**, 760–763.

Charlier, D., Hassanzadeh, G., Kholti, A., Gigot, D., Pierard, A., and Glansdorff, N. 1995. carP, involved in pyrimidine regulation of the *Escherichia coli* carbamoylphosphate synthetase operon encodes a sequence-specific DNA-binding protein identical to XerB and PepA, also required for resolution of ColEI multimers. *J. Mol. Biol.* **250**, 392–406.

Delano, W.L. 2002. The PyMOL User's Manual.

Doan, T.T., Kim, J.K., Kim, H., Ahn, Y.J., Kim, J.G., Lee, B.M., and Kang, L.W. 2008. Expression, crystallization and preliminary X-ray crystallographic analysis of Xoo0352, D-alanine-D-alanine ligase A, from *Xanthomonas oryzae* pv. *oryzae*. *Acta. Crystallogr. Sect. F Struct. Biol. Cryst. Commun.* **64**, 1115–1117.

Emsley, P. and Cowtan, K. 2004. Coot: model-building tools for molecular graphics. *Acta. Crystallogr. D Biol. Crystallogr.* **60**, 2126–2132.

Huynh, K.H., Natarajan, S., Choi, J., Song, N.H., Kim, J.G., Lee, B.M., Ahn, Y.J., and Kang, L.W. 2009. Cloning, expression, crystallization and preliminary X-ray crystallographic analysis of leucine aminopeptidase (LAP) from the *pepA* gene of *Xanthomonas oryzae* pv. *oryzae*. *Acta. Crystallogr. Sect. F Struct. Biol. Cryst. Commun.* **65**, 952–955.

Kim, S.H., Lee, S.E., Hong, M.K., Song, N.H., Yoon, B., Viet, P., Ahn, Y.J., Lee, B.M., Jung, J.W., Kim, K.P., and *et al.* 2011. Homologous expression and quantitative analysis of T3SS-dependent secretion of TAP-tagged XoAvrBs2 in *Xanthomonas oryzae* pv. *oryzae* induced by rice leaf extract. *J. Microbiol. Biotechnol.* **21**, 679–685.

Kim, S., Nguyen, T.D., Lee, J., Hong, M.K., Pham, T.V., Ahn, Y.J., Lee, B.M., Han, Y.S., Kim, D.E., Kim, J.G., and Kang, L.W. 2013. Homologous expression and T3SS-dependent secretion of TAP-tagged Xo2276 in *Xanthomonas oryzae* pv. *oryzae* induced by rice leaf extract and its direct *in vitro* recognition of putative target DNA sequence. *J. Microbiol. Biotechnol.* **23**, 22–28.

Kraft, M., Schleberger, C., Weckesser, J., and Schulz, G.E. 2006. Binding structure of the leucine aminopeptidase inhibitor microginin FR1. *FEBS Lett.* **580**, 6943–6947.

Laskowski, R., MacArthur, M., Moss, D., and Thornton, J. 1993. PROCHECK: a program to check the sterochemical quality of protein structures. *J. Appl. Cryst.* **26**, 283–291.

Lee, B.M., Park, Y.J., Park, D.S., Kang, H.W., Kim, J.G., Song, E.S., Park, I.C., Yoon, U.H., Hahn, J.H., Koo, B.S., and *et al.* 2005. The genome sequence of *Xanthomonas oryzae* pathovar *oryzae* KACC10331, the bacterial blight pathogen of rice. *Nucleic Acids Res.* **33**, 577–586.

Lu, J.P., Yuan, X.H., and Ye, Q.Z. 2012. Structural analysis of inhibition of *Mycobacterium tuberculosis* methionine aminopeptidase by bengamide derivatives. *Eur. J. Med. Chem.* **47**, 479–484.

Matsui, M., Fowler, J.H., and Walling, L.L. 2006. Leucine aminopeptidases: diversity in structure and function. *Biol. Chem.* **387**, 1535–1544.

Murshudov, G.N., Vagin, A.A., and Dodson, E.J. 1997. Refinement of macromolecular structures by the maximum-likelihood method. *Acta. Crystallogr. D Biol. Crystallogr.* **53**, 240–255.

Neumann, U., Forchert, A., Flury, T., and Weckesser, J. 2006. Microginin FR1, a linear peptide from a water bloom of *Microcystis* species. *FEMS Microbiol. Lett.* **153**, 475–478.

Otwinowski, Z. and Minor, W. 1997. Processing of X-ray diffraction data collected in oscillation mode. *Methods Enzymol.* **277**, 307–326.

Payne, D.J., Gwynn, M.N., Holmes, D.J., and Pompliano, D.L. 2007. Drugs for bad bugs: confronting the challenges of antibacterial discovery. *Nat. Rev. Drug Discov.* **6**, 29–40.

Rawlings, N.D. and Barrett, A.J. 1996. *Methods Enzymol.* **248**, 183–228.

Rawlings, N.D., Morton, F.R., and Barrett, A.J. 2006. MEROPS: the peptidase database. *Nucleic Acids Res.* **34**, D270–272.

Reijns, M., Lu, Y., Leach, S., and Colloms, S.D. 2005. Mutagenesis of PepA suggests a new model for the *Xer/cer* synaptic complex. *Mol. Microbiol.* **57**, 927–941.

Sivaraman, K.K., Oellig, C.A., Huynh, K., Atkinson, S.C., Poreba, M., Perugini, M.A., Trenholme, K.R., Gardiner, D.L., Salvesen, G., Drag, M., and *et al.* 2012. X-ray crystal structure and specificity of the *Plasmodium falciparum* malaria aminopeptidase PfM18AAP. *J. Mol. Biol.* **422**, 495–507.

Stirling, C.J., Colloms, S.D., Collins, J.F., Szatmari, G., and Sherratt, D.J. 1989. *xerB*, an *Escherichia coli* gene required for plasmid ColE1 site-specific recombination, is identical to *pepA*, encoding aminopeptidase A, a protein with substantial similarity to bovine lens leucine aminopeptidase. *EMBO J.* **8**, 1623–1627.

Strater, N., Sherratt, D.J., and Colloms, S.D. 1999. X-ray structure of aminopeptidase A from *Escherichia coli* and a model for the nucleoprotein complex in Xer site-specific recombination. *EMBO J.* **18**, 4513–4522.

Taylor, A. 1993. Aminopeptidase: structure and function. *FASEB J.* **7**, 290–298.

Vagin, A. and Teplyakov, A. 2010. Molecular replacement with MOLREP. *Acta Crystallogr. D Biol. Crystallogr.* **66**, 22–25.

Zhang, H. and Wang, S. 2013. Rice versus *Xanthomonas oryzae* pv. *oryzae*: a unique pathosystem. *Curr. Opin. Plant Biol.* **16**, 188–195.